Dalton Transactions

Accepted Manuscript

ROYAL SOCIETY OF CHEMISTRY

www.rsc.org/dalton

Journal Name

RSCPublishing

ARTICLE

High-Pressure Phase Transitions in Ordered and Disordered Bi_2Te_2Se

Cite this: DOI: 10.1039/x0xx00000x

M. B. Nielsen,[a] P. Parisiades,[b] S. R. Madsen[a] and M. Bremholm[a]

Received 00th January 2012,
Accepted 00th January 2012

DOI: 10.1039/x0xx00000x

www.rsc.org/

We report studies of pressure-induced phase transitions of ordered and disordered ternary tetradymite-like Bi_2Te_2Se by synchrotron powder x-ray diffraction (PXRD) in diamond anvil cells (DACs) for pressures up to 59 and 49 GPa, respectively. The first sample (SB) was prepared from a single crystal with ordered Se/Te sites while the second sample (Q) was prepared from a quenched melt resulting in disordered Se/Te. This allows for an investigation of the effect of disorder on the phase transitions and the equation of states (EoS) of the tetradymite-like α phase. Fitting of a third order Birch-Murnaghan EoS to the α phases yielded bulk moduli K_0 of 34.5(10) and 38.3(17) GPa and K' of 6.2(3) and 5.0(5) for the SB and Q samples, respectively. An electronic topological transition (ETT) was identified in both samples at pressures of 4.4 and 3.1 GPa, respectively. This was followed by a transition near 11 GPa to a phase that is isostructural with the β phase of Bi_2Te_3. The Se/Te ordering only affects the transition pressure to a small extent. A cubic phase that resembles the δ phase observed in high-pressure studies of Bi_2Te_3 appears at 17-20 GPa, but the ternary composition leads to a more complex structure. The presence of a low angle diffraction peak in the δ phase demonstrates that the true structure is not simply body-centred cubic. In this way the samples resemble Bi_2Se_3 where Bi and Se show a high degree of ordering, but the proposed structure of δ-Bi_2Se_3 also does not fully describe the data for δ-Bi_2Te_2Se.

1. Introduction

Bi_2Se_3 and Bi_2Te_3 have the same crystal structure and form a solid-solution $Bi_2Se_{3-x}Te_x$ ($0 \leq x \leq 3$). The end members and the ternaries have been studied intensely for decades owing to their excellent thermoelectric properties.[1] More recently, the interest has been further invigorated as these compounds were predicted and confirmed to be topological insulators.[2] The link between thermoelectricity and the topologically protected surface states has been established very recently for Bi_2Te_3 and Bi_2Te_2Se (x = 1).[3] Stoichiometric Bi_2Se_3 is an intrinsic n-type semiconductor due to Se vacancies ($V_{Se}^{\bullet\bullet}$) while stoichiometric Bi_2Te_3 is a p-type semiconductor due to antisite defects (i.e. Bi'_{Te}).[4] Bi_2Te_2Se is a particularly interesting stoichiometry because for $x \approx 1$ the two primary defect types are compensated and a p-n transition is observed. It follows that very low carrier concentrations can be obtained in this region.[5] Furthermore, x = 1 is also a special case as Bi_2Te_2Se is the only composition where the layers that only have Bi as closest neighbors are fully occupied by Se while Te caps the quintuple layers (Fig. 1a) resulting in the tetradymite structure type. However, the ordering requires very stable growth conditions as the energies required to form both Te_{Se} and Te_{Bi} antisite defects are very low.[3-4, 6] This means that a crystal with disordered Se and Te can be obtained by quenching Bi_2Te_2Se from the melt. The space group for the tetradymite structure is $R\bar{3}m$ (Z = 3) and for the ordered case of Bi_2Te_2Se the Se is located on the 3a site.

For the end members a number of interesting phase transitions appear at high pressure. Prior to any structural transition an electronic topological transition (ETT) is observed in the α phase.[7] This is followed by three phase transitions in the case of Bi_2Te_3. Although the pressure-induced phase transitions were first observed in Bi_2Te_3 several decades ago,[8] it was only recently that structures of these were actually solved. The first pressure-induced phase transition results in a monoclinic phase (space group $C2/m$, referred to as the β phase, shown in Fig. 1b). The structure was solved relatively recently[9] and is similar to the α phase with the exception that Te-Te distances from neighboring layers are now so short that Te is coordinated to Bi in both quintuple layers. In the same paper, theoretical calculations predicted an additional monoclinic γ phase and the PXRD data matched this phase in a narrow pressure range (14-15 GPa).[9-10] At the highest pressure Bi_2Te_3 undergoes one more phase transition to a cubic δ phase (space group $Im\bar{3}m$), where it forms a solid solution substitutional alloy with no apparent ordering of Bi and Te.[9-10] The coordination of Bi and Te is eight-fold and this structure

persists to the highest pressures that have been investigated. The unit cell is shown in Figure 1c.

Substitutional alloys can form when atoms are approximately the same size and have nearly the same electronegativity as described by the Hume-Rothery rules.[11] Therefore it may at first appear surprising that Bi_2Te_3 should form such an alloy at high pressure since at ambient conditions the ionic radius of Bi^{3+} is 117 pm while Te^{2-} is 207 pm.[12] However, when high pressure is applied the situation changes drastically, and the sizes of the two ions are observed to become similar above approx. 20 GPa due to charge transfer from Te to Bi.[9]

The full high-pressure phase behavior of Bi_2Se_3 is still a matter of debate, with some reports that the high-pressure phases follow the sequence $R\bar{3}m \rightarrow C2/m \rightarrow I4/mmm$ with pressure,[13] while others report the sequence $R\bar{3}m \rightarrow C2/m \rightarrow C2/c \rightarrow C2/m$[14] and yet others suggest $R\bar{3}m \rightarrow C2/m \rightarrow C2/c \rightarrow Im\bar{3}m$, here noting that the last phase is inferred only from a lack of active Raman modes which should be present in a monoclinic cell.[15] That Bi_2Se_3 might be less willing to form a substitutional alloy with respect to Bi_2Te_3 can be recognized from the fact that while the electronegativities of Bi and Te are quite similar (2.02 and 2.10 on the Pauling scale[16]), while that of Se is significantly higher at 2.55.

In the present study we investigate the high-pressure structural changes in two different samples of approximate Bi_2Te_2Se composition, the first highly ordered in Se/Te while the second sample has completely disordered Se/Te. This allows for an investigation of the effect of disorder on the first phase transition and the equation of state (EoS) of the tetradymite α phase. We also report the EoS of the high-pressure phases of Bi_2Te_2Se and comment on the still uncertain nature of the δ phase.

2. Experimental

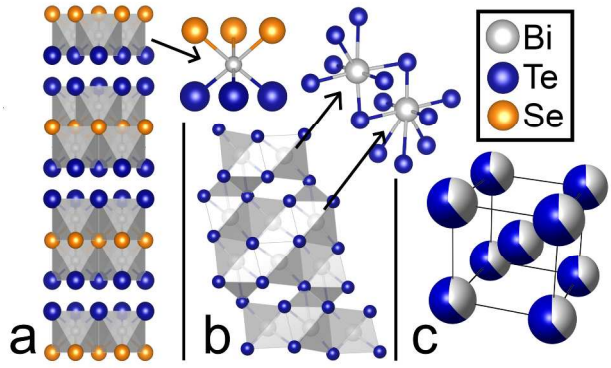

Figure 1. a) The α-Bi_2Te_2Se unit cell with six-fold Bi coordination. b) The β-Bi_2Te_3 structure displaying seven- and eight-fold Bi coordination. This structure is basically the α-phase with Bi-Te bonding reaching through the Te-layers. c) The δ-Bi_2Te_3 structure where Bi and Te are completely disordered over the sites. The coordination for both is eight-fold.

2.1 Sample synthesis

Large single crystals with a nominal composition of Bi_2Te_2Se were prepared by the Stockbarger-Bridgman method as described in detail elsewhere.[5] A fine powder was obtained by using a diamond file at a point where the composition was $Bi_2Te_{1.75}Se_{1.19}$, coinciding with the p-n transition where the sample conductivity is lowest. This sample is referred to as the Stockbarger-Bridgman (SB) sample.

A sample of composition Bi_2Te_2Se was made by sealing stoichiometric amounts of the elements in an evacuated quartz ampule, heating to above the melting point and rapidly quenching in ice water. A fine powder was obtained by using a diamond file on the large polycrystal. This sample is referred to as the quenched (Q) sample.

In both cases the fine powder was dispersed in ethanol and allowed to settle briefly before the remaining suspended particles were transferred to a new vial. This process was repeated several times in order to obtain only very small grains of the samples. The ethanol was then evaporated at 60 °C. Following this floating procedure, small amounts of powder were pressed into foils of 10-15 μm thickness by placing the powders between the faces of two 600 μm diamond anvils and pressing them together by hand. The foils were then subsequently transferred to the diamond anvil cell sample chambers.

2.2 High pressure diamond anvil experiments

Powder x-ray diffraction (PXRD) as a function of pressure was carried out at ID27 at the European Synchrotron Radiation Facility (ESRF)[17], using a wavelength of 0.3738(2) Å. The samples were loaded in membrane driven diamond anvil cells (DACs) with 300 μm culets. The pressure-transmitting medium was neon loaded using a gas-loading system (Sanchez Technologies GLS1500). A 250 μm thick Re gasket was pre-indented to an initial thickness of about 40 μm after which a circular hole was laser-cut in the center of the indentation with a diameter of approximately 3/5 the culet size. A small foil of pressed Cu powder was loaded together with a ruby crystal as the pressure standards. The pressures were calculated using the Cu EoS by Dewaele *et al.*[18] (Vinet EoS, K_0 = 132.4(14) GPa, K_0' = 5.32(6)) with our V_0 = 47.405(2) Å^3 (unit cell volume).

2.3 Calibration and refinements

The PXRD setup was calibrated using a LaB_6 standard (NIST SRM 660b). The 2D data obtained from the detector were all treated using the program MAUD[19] following the guidelines by Lutterotti *et al.*[20] and Wenk *et al.*[21]

The sample 2D data sets were sectioned in 10 degree azimuthal slices, allowing the refinement of anisotropic strain parameters as well as texture. The arbitrary texture setting in MAUD is the 2D equivalent of a Le Bail refinement[22] and was in most cases used to account for intensity variation of the Debye-Scherrer rings along the azimuth as this allows a more accurate determination of the unit cell parameters than a full Rietveld refinement.

The refined parameters were: Incident intensity, vertical and horizontal beam center correction, unit cell parameters, crystallite size and root mean square micro-strain (using the Delft model in MAUD[20]).

The SB sample comes into contact with both diamond anvils at a pressure of approx. 20 GPa. This is typically referred to as bridging and is inferred from the sudden onset of strong anisotropic strain that is only present in the sample (2D data clearly showing this is shown in the Supporting Information, Fig. S1) but not in the Ne pressure medium or in the Cu calibrant. The anisotropic strain was modelled using three off-diagonal macro-stress parameters using the Moment Pole Stress model[23] in MAUD with a 0.5 Voigt-Reuss weight and the BulkPathGeo formulation.[23] This model accounts for anisotropic deformation of the sample. To get a quantitative interpretation of the macro-stress parameters one would need to know the elasticity tensor of the sample. Since these constants are not available for the δ-phase of Bi_2Te_2Se this was not attempted and the (arbitrary) default values of MAUD were used to simply describe the observed strains.

Full Rietveld refinements were carried out in the δ phase using an isotropic *B*-value that was constrained to be identical for all atoms.

2.4 Equation of state fitting

The volume versus pressure data obtained from the refinements in MAUD were fitted to their respective EoS using EoSFit7.[24] The third order Birch-Murnaghan (BM3) EoS (equation 1) was used where possible, while the second order (BM2) ($K_0' = 4$) was used if the BM3 did not significantly improve the fit.

$$P(V) = 3K_0 f_E(1+2f_E)^{5/2}\left(1+\tfrac{3}{2}(K_0'-4)f_E\right) \qquad (1)$$

where $f_E = \left((V_0/V)^{2/3}-1\right)/2$

For the high pressure phases a reference bulk modulus and first derivate, K_R and K_R' were used instead of K_0 and K_0'. The bulk modulus and its pressure derivative obtained from fitting the EoS with a reference pressure thus refer to the values where the phase is first observed, rather than the hypothetical zero pressure values. By using K_R and K_R' large uncertainties resulting from extrapolation to zero pressure are thus avoided. Identical reference pressures were chosen for the β phases (11.8 GPa) and δ phases (19.5 GPa) for the two samples in order to facilitate comparison.

3. Results and discussion

3.1 Phase transitions

The low angle region of the integrated data sets from the SB and Q samples displaced with increasing pressure can be seen in Fig. 2. The full data extend to 30° in 2θ, while most refinements have been carried out using data to 24°. Large plots of all datasets in the full angular range are supplied in the Supporting Information, Fig. S2 and S3.

The samples investigated both undergo at least two structural phase transitions as pressure is increased, as is clear from Fig. 2a and 2b. The observed pattern after the first transition resembles that of the Bi_2Te_3 β phase and can be indexed using the same symmetry (*C*2/*m* unit cell). The first transition, from α to β ($R\bar{3}m$ to *C*2/*m*), is first observed at 11.4 and 10.9 GPa in the SB and Q samples respectively, with the monoclinic β phase being phase-pure at 14.4 and 12.6 GPa. The second transition observed is from the β phase to a cubic δ phase (discussed further in section 3.4) and has its onset at 19.6 and 16.7 GPa, with completion at 21.2 and 22.0 GPa for the two samples. Weak diffraction near 9° 2θ in the Q sample (Fig. 2b) matches the *C*2/*c* phase which has been reported in Bi_2Se_3[14-15] and Bi_2Te_3,[9, 10b, 25] but the data quality precluded stable refinements of this phase. In the SB sample, strong Re

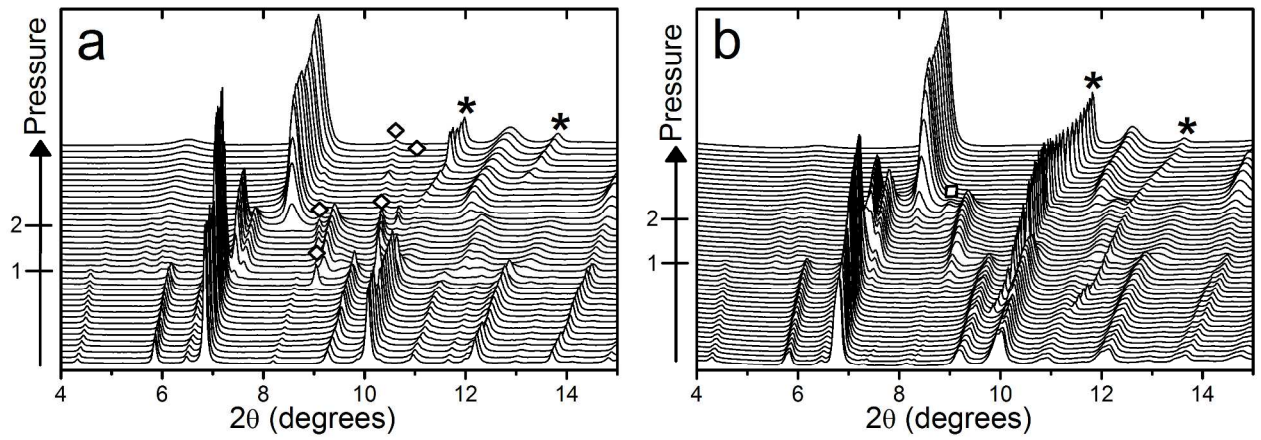

Figure 2. a) Integrated angular diffraction data on the SB sample displaced with increasing pressure (not to scale). For clarity and due to the high number of datasets, only every second dataset is plotted here. The first phase transition at 11.4 GPa is marked with 1, while 2 marks the second onset at 19.6 GPa. b) Integrated angular diffraction data on the Q sample with increasing pressure (not to scale). The first phase transition at 10.9 GPa is marked with 1, while 2 marks the second onset at 16.7 GPa. The square in (b) marks the position of a cluster of peaks that fit the γ Bi_2Te_3 type structure. The diamond marks diffraction from rhenium while asterisks mark Ne. The final pressure in (a) is 58.7(5) and 48.9(4) GPa in (b).

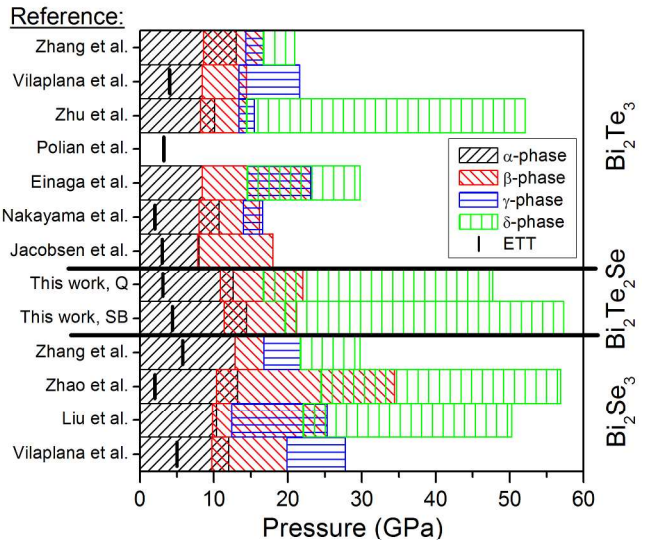

Figure 3. Comparison of the ranges of stability from experiments reported in literature for Bi_2Te_3, this work and Bi_2Se_3. In each case, the upper limit shows the maximum reported pressure in that study, not necessarily the upper stability limit.

scattering is present, with one major reflection overlapping in position with the positions of the γ phase. This prevents us from making definite statements of its presence in this sample. As in other studies that report this phase it is not observed pure at any pressure (it always coexists with the β or δ phase). It should also be mentioned that some studies on Bi_2Se_3 do not observe it at all.[13]

The reported pressure ranges for the various transitions in the two end members also vary somewhat in literature, as can be seen in Fig. 3. Our observed transition pressures are closest to those reported for Bi_2Se_3, both for the α → β transition and (presence of a *C*2/*c* phase or not) for the range where the last phase appears (termed the β → δ transition here).

3.2 Refinement results

Unit cell volumes of the three phases normalized to one formula unit are plotted in Fig. 4a and 4b for the SB and Q samples respectively. These volumes were all extracted using the arbitrary texture setting in MAUD, i.e. 2D Le Bail fitting. This method leads to satisfactory fits as long as the amount of peak overlap is not too large. The reported volumes are all from data sets that gave stable refinements. The refined unit cell parameters at the various pressures are given in the Supporting Information, Table ST1.

The evolutions of the *c*/*a* ratios in the α phase versus pressure for the two samples are plotted in Fig. 5. The *a*- and *c*-axis lengths were extracted using the arbitrary texture setting of MAUD. The ratio drops relatively quickly during the first few GPa indicating that the *c*-direction is more easily compressed. Near 3 GPa the trend reverses and a slow increase in the ratio is seen, indicating that the *ab*-plane is now more easily compressed than the *c*-direction.

From these changes it is inferred that both samples undergo an isostructural pressure-induced electronic topological transition (ETT) at pressures of about 3.1 GPa for the Q sample and about 4.4 GPa for the SB sample. This transition in the α phase is also observed at similar pressures for Sb_2Te_3, Bi_2Se_3 and Bi_2Te_3 (see Fig. 2 of ref. 7). This second order isostructural transition appears because the compressibility along the c-axis suddenly drops by a large amount. From a band-structure point of view, the isostructural transition is a symptom of a large rearrangement of the electronic density of states at the Fermi energy. The rearrangement occurs when a Van Hove singularity crosses the Fermi energy.[7, 26] A more general chemical viewpoint would be to infer covalent bond-formation between the Te atoms of the adjacent quintuple layers since the Te-Te distances now become so short that they no longer only interact via van der Waals forces.

Rietveld refinements of the β phase of both samples did not enable us to conclude if Se shows a preference for any particular of the three chalcogenide sites in the monoclinic cell.

3.3 Equations of state

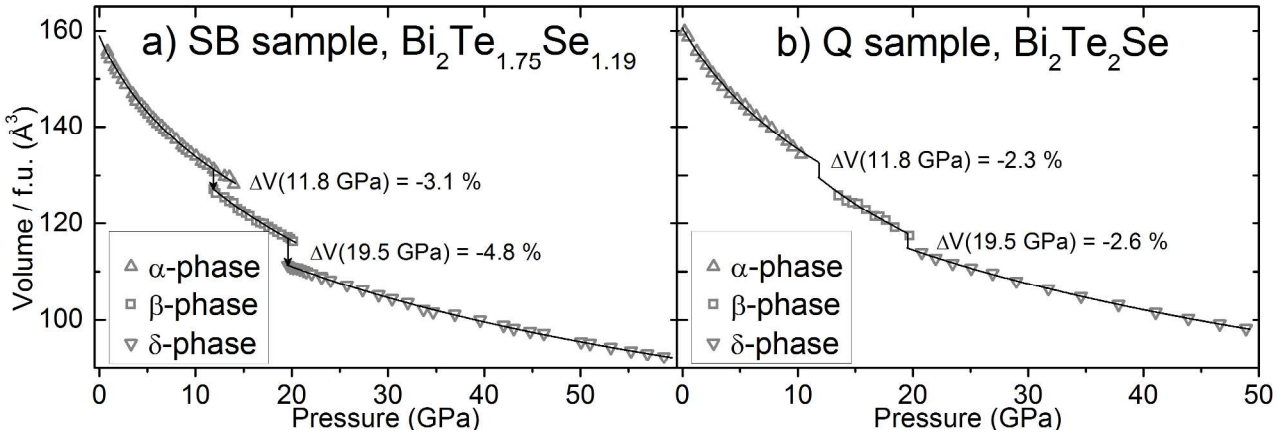

Figure 4. Symbols: Experimental volume per formula unit versus pressure. Solid lines: Fitted equation of state for each respective phase. Pressure and volume error bars are smaller than the symbols. Note that the pressure scales are different while the volume axes are identical. a) SB sample results. b) Q sample results.

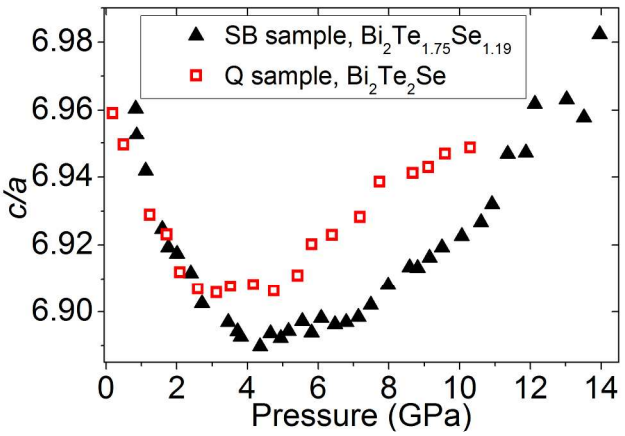

Figure 5. *c*/*a* ratio of the α-phase unit cell versus pressure. Triangles mark the SB sample while squares mark the Q sample. Error bars are smaller than the symbols.

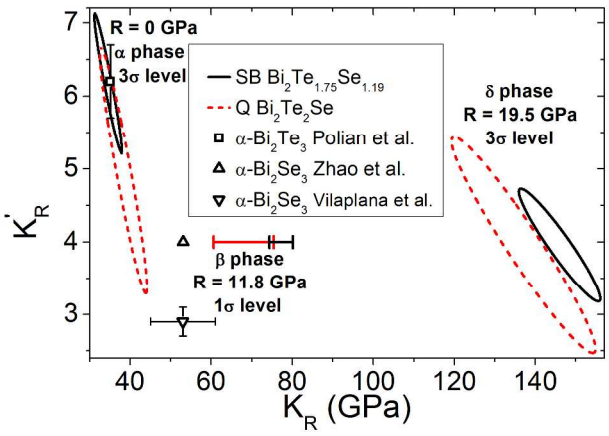

Figure 6. The results of fitting BM3 equations of state to the α- and δ-phases (ellipses) and a BM2 to the β-phase (horizontal error bars) along with reported experimental results on the end members in the α phase. R refers to the reference pressure of each EoS fit. Black solid lines represent the SB sample; red dashed lines the Q sample.

The results of fitting a BM3 EoS to the α and δ phases, along with a fit of a BM2 EoS to the β phase are shown in Fig. 6, as 3σ confidence ellipses in K and K' for the BM3 fits and as 1σ error bars at $K' = 4$ for the BM2 fit.[27] The pressure value R refers to the reference pressure of each EoS fit, chosen as the first pressure where the phase in question appears. A full list of V_R, K_R, K'_R and changes in V and K at the transition points is supplied in Table 1. Literature values of BM2 and BM3 fits to experimental data on α-Bi_2Se_3 and α-Bi_2Te_3 are included in Fig. 6 as symbols.[13, 15, 28] No error bar means that the reported uncertainty in that parameter is less than the size of the symbol.

The EoS parameters were obtained by least-square fitting to the weighted P,V data. When two phases coexist, only the majority phase from stable refinements was used. The bulk modulus of the α phase, being identical within the uncertainty for the SB and Q samples, does not seem to depend on stoichiometry or initial ordering of the Se/Te atoms, indicating that both the intra- and interlayer interactions do not depend on the Se/Te order initially. When comparing to experimental results reported in literature on the pure compounds it is seen that there is no significant difference between the obtained EoS values of the two samples and those reported for pure Bi_2Te_3,[28] while the values reported by others for Bi_2Se_3 show significantly higher values of K_0.[13, 15]

The changes in volume and bulk modulus at each reference transition point are shown in Table 1. The volume drop at each transition is larger for the SB sample with its higher Se content, but overall the two samples show quite similar behavior.

If the volume of the SB sample in the β phase is extrapolated to zero pressure it yields V_0 = 164(3) Å^3 (Q sample extrapolation is too uncertain to provide meaningful results). When compared to the reported extrapolations for Bi_2Se_3 (V_0 = 132.3(5) Å^3, fit of experiment)[15] and Bi_2Te_3 (V_0 = 161.99 Å^3, fit of theory)[29] it corroborates several reports of deviations from Vegard's rule in these systems at both ambient and high pressure.[10a, 30]

It is interesting that the δ phases show significant differences in EoS parameters in spite of similar stoichiometry. The structural properties at these pressures clearly depend strongly on the Se content and it is perhaps not surprising that Se must be the dominant factor since Bi and Te behave sufficiently alike to form a disordered alloy in the pure telluride. That the bulk modulus of the SB sample is higher shows that the interactions of Se with its local environment must be stronger than those of Te (since they resist compression more).

3.4 The nature of the δ phase

While Bi_2Te_3 forms a disordered bcc alloy there are differing reports about the structure Bi_2Se_3 at the highest pressures.[13-15] Fig. 7a shows a dataset from the Q sample at 47.7(4) GPa, along with a Rietveld refinement using an $Im\bar{3}m$ cell with a random distribution of the three elements, like that observed for Bi_2Te_3. The peak observed at 6.4° 2θ is forbidden by the space group. The SB sample at 48.8(4) GPa shows the same low

Table 1. Equation of state model parameters for all three phases of the SB and Q samples. Volumes unit is Å^3, pressure and K unit is GPa, K' is unitless.

SB sample, $Bi_2Te_{1.75}Se_{1.19}$				Q sample, Bi_2Te_2Se			
$V_R(\alpha)$ =	158.92(18)	$P_R(\alpha)$ =	0	$V_R(\alpha)$ =	160.6(2)	$P_R(\alpha)$ =	0
$K_R(\alpha)$ =	34.5(10)	$K'_R(\alpha)$ =	6.2(3)	$K_R(\alpha)$ =	38.3(17)	$K'_R(\alpha)$ =	5.0(5)
$\Delta V_R(\alpha/\beta)$ =	-4.0(2)	$\Delta K_R(\alpha/\beta)$ =	-20(3)	$\Delta V_R(\alpha/\beta)$ =	-3.1(8)	$\Delta K_R(\alpha/\beta)$ =	-23(7)
$V_R(\beta)$ =	127.3(2)	$P_R(\beta)$ =	11.8	$V_R(\beta)$ =	129.6(8)	$P_R(\beta)$ =	11.8
$K_R(\beta)$ =	77(3)	$K'_R(\beta)$ =	4 (fixed)	$K_R(\beta)$ =	68(7)	$K'_R(\beta)$ =	4 (fixed)
$\Delta V_R(\beta/\delta)$ =	-5.6(2)	$\Delta K_R(\beta/\delta)$ =	39(3)	$\Delta V_R\beta/\delta)$ =	-3.1(4)	$\Delta K_R(\beta/\delta)$ =	40(8)
$V_R(\delta)$ =	111.42(6)	$P_R(\delta)$ =	19.5	$V_R(\delta)$ =	114.9(1)	$P_R(\delta)$ =	19.5
$K_R(\delta)$ =	146(3)	$K'_R(\delta)$ =	4.0(2)	$K_R(\delta)$ =	137(5)	$K'_R(\delta)$ =	4.0(4)

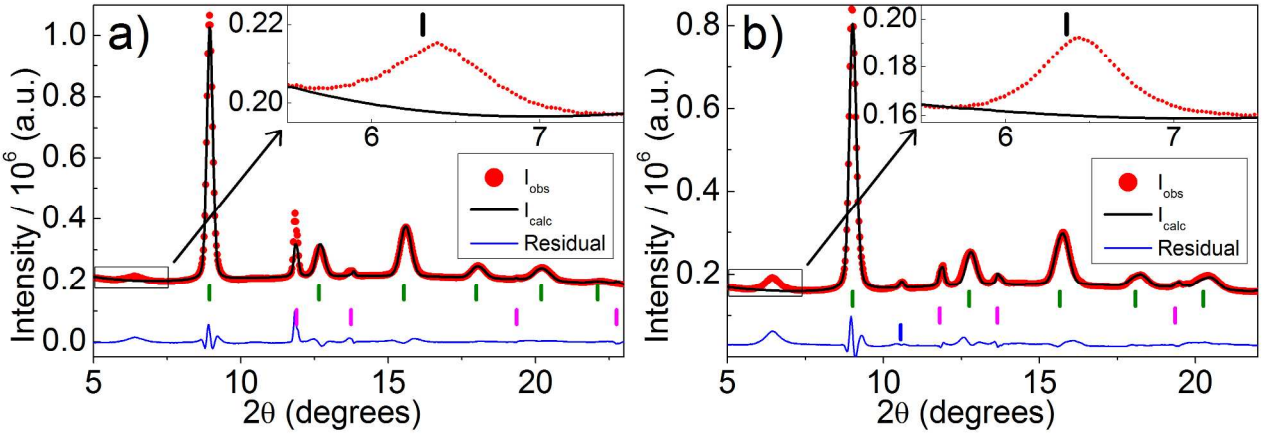

Figure 7. Rietveld refinement of a) the Q sample and b) the SB sample, both in the δ-phase. Red dots are data, black line is the fit, blue line is the difference, green bars (top row) indicate Bragg positions of the bcc cell, pink bars (second row) indicate Bragg positions of Ne and blue bar (third row) indicates Bragg position of Re. Insets: Zoom on the low angle data. Black bar indicates where the (100) peak would be located if it was allowed.

angle peak in the δ phase with even greater relative intensity, Fig. 7b. The peak nearly coincides with the forbidden {100} but is both shifted to a higher angle and is significantly broadened.

The difference between the unit cell obtained by a bcc model and a hypothetical unit cell length a_{100} obtained from a single peak fitting does not depend significantly on pressure for the SB sample while the Q sample displays a significant negative slope with pressure (the peak moves towards the cubic value).

The low angle peak is also much wider than what would be expected from a simple symmetry breaking from bcc to a primitive cubic cell and the width of the low angle peak increases with pressure compared to the main δ phase peak widths. At the same time the intensity of the low angle peak normalized to the (110) peak intensity (the main bcc peak) as a function of pressure does not seem to depend on pressure when the uncertainties are taken into consideration.

The unexplained peak shows strain identical to the δ phase peaks when observed in the 2D data (see Supporting Information, Fig. S1). As the elastic tensor of a material and thus its response to macro stress is a product of structure and chemical identity, this indicates that the unexplained peak is not caused by an impurity, but originates from the δ phase.

An exhaustive search for a model that predicts the (100) peak and no further reflections has not been successful. The main reason for this is that the low angle peak is the only additional peak observed. A number of models have been attempted, including the *I4/mmm* cell proposed by Zhao *et al.* for Bi_2Se_3, but none provide a satisfactory explanation of the data. We can therefore only conclude that the δ phase of Bi_2Te_2Se is more complex than δ-Bi_2Te_3 but also different from δ-Bi_2Se_3. The models and their fits are given in the Supporting Information, Figures S4-6.[13]

4 Conclusion

The topological insulator Bi_2Te_2Se with two slightly different compositions has been investigated up to a pressure of 59 GPa. Both samples show indications of an electronic topological phase transition at 3-4 GPa in the α phase, followed by two structural phase transitions near 11 and 19 GPa into the β and δ phases. The β phase was found to have the same structure as that observed for Bi_2Se_3 and Bi_2Te_3, though whether Se and Te are disordered over the available sites in the monoclinic cell proved to be beyond the data to resolve. Hints of the intermediate monoclinic γ phase were observed in the Q sample, but it was not possible to refine this structure.

EoS parameters for the α, β and δ phases were reported for both samples. The values of the α phase parameters are identical with those reported in the literature for Bi_2Te_3. At high pressure the EoS parameters show significant dependence on the Se-content of the sample.

The structure of the δ phase is close to body-centered cubic, but the presence of a low angle peak violates the symmetry of this simple model. Exhaustive attempts at building a simple model that predicts only the very wide low angle peak and no further reflections were unsuccessful. It would be interesting to see if a Monte Carlo simulation of a large unit cell at these high pressures could provide some insight into the short-range ordering of Se/Te. We consider it likely that Bi/Te atoms are (almost) completely disordered in the structure, while Se (being the anion with largest negative charge) probably disfavors like neighbors and might also prefer Bi over Te as closest neighbor due to the (small) positive charge on the former. This would also be a relevant question for a theoretical study. Overall, the behavior of Bi_2Te_2Se (in the δ phase) is dominated by the presence of Se, both in the structural transition pressures, EoS parameters in the δ phase and in the structure of the δ phase itself. The reason for this dominance is probably that Se is both the largest ion and has the greatest (negative) charge at the pressures where this phase dominates, while Bi and Te seem to behave almost identically at these pressures.

Acknowledgements

The ID27 beamline staff at ESRF is gratefully acknowledged for access to beamtime. DanScatt is thanked for financial support for travel expenses for beamtimes. MB thanks the Villum Foundation and CMC for funding. CMC is a Center of Excellence funded by the Danish National Research Foundation (DNRF93).

Notes and references

[a] Center for Materials Crystallography (CMC), Department of Chemistry and iNANO, Aarhus University, Langelandsgade 140, 8000 Aarhus C, Denmark.

[b] European Synchrotron Radiation Facility (ESRF), Beamline ID27, 71 Avenue des Martyrs, CS 40220, 38043, Grenoble Cedex 9, France.

Electronic Supplementary Information (ESI) available: 2D integrated dataset plot (Fig. S1), Full diffraction raw data set plots (Fig. S2 and S3), Refinement result tables for both phases at all pressures (Table ST1), attempted refinement models for the δ phase (Fig. S4-6). See DOI: 10.1039/b000000x/

1 G. J. Snyder, E. S. Toberer, *Nat. Mater.* 2008, ***7***(2), 105-114.
2 M. Z. Hasan, C. L. Kane, *Rev. Mod. Phys.* 2010, **82**(4), 3045-3067.
3 H. Shi, D. Parker, M. Du, D. J. Singh, *Phys. Rev. Appl.* 2015, ***3***(1), 014004(1-10).
4 L.-L. Wang, M. L. Huang, S. Thimmaiah, A. Alam, S. L. Bud'ko, A. Kaminski, T. A. Lograsso, P. Canfield, D. D. Johnson, *Phys. Rev. B* 2013, ***87***(12), 125303(1-6).
5 J. L. Mi, M. Bremholm, M. Bianchi, K. Borup, S. Johnsen, M. Sondergaard, D. D. Guan, R. C. Hatch, P. Hofmann, B. B. Iversen, *Adv. Mater.* 2013, ***25***(6), 889-893.
6 D. West, Y. Y. Sun, H. Wang, J. Bang, S. B. Zhang, *Phys. Rev. B* 2012, ***86***(12), 121201(R)(1-4).
7 F. J. Manjon, R. Vilaplana, O. Gomis, E. Perez-Gonzalez, D. Santamaria-Perez, V. Marin-Borras, A. Segura, J. Gonzalez, P. Rodriguez-Hernandez, A. Munoz, C. Drasar, V. Kucek, V. Munoz-Sanjose, *Phys. Status Solidi B* 2013, ***250***(4), 669-676.
8 (a) L. F. Vereshch, N. A. Bendelia, E. Y. Atabaeva, *Sov. Phys. - Solid State* 1972**,** ***13***(8), 2051-2053; (b) M. A. Il'ina, E. S. Itskevich, *Sov. Phys. - Solid State* 1972, ***13***(8), 2098-2100.
9 L. Zhu, H. Wang, Y. C. Wang, J. A. Lv, Y. M. Ma, Q. L. Cui, Y. M. Ma, G. T. Zou, *Phys. Rev. Lett.* 2011, ***106***(14), 145501(1-4).
10 (a) M. Einaga, A. Ohmura, A. Nakayama, F. Ishikawa, Y. Yamada, S. Nakano, *Phys. Rev. B* 2011, ***83***(9), 092102(1-4); (b) S. J. Zhang, J. L. Zhang, X. H. Yu, J. Zhu, P. P. Kong, S. M. Feng, Q. Q. Liu, L. X. Yang, X. C. Wang, L. Z. Cao, W. G. Yang, L. Wang, H. K. Mao, Y. S. Zhao, H. Z. Liu, X. Dai, Z. Fang, S. C. Zhang, C. Q. Jin, *J. Appl. Phys.* 2012, ***111***(11), 112630(1-6).
11 W. Hume-Rothery, G. V. Raynor, in *The Structure of Metals and Alloys*, Institute of Metals Press: London, U.K., 1969.
12 R. D. Shannon, *Acta Crystallogr., Sect. A* 1976, ***32***(Sep1), 751-767.
13 J. G. Zhao, H. Z. Liu, L. Ehm, D. W. Dong, Z. Q. Chen, G. D. Gu, *J. Phys.: Condens. Matter* 2013, ***25***(12), 125602(1-8).
14 G. T. Liu, L. Zhu, Y. M. Ma, C. L. Lin, J. Liu, Y. M. Ma, *J. Phys. Chem. C* 2013, ***117***(19), 10045-10050.
15 R. Vilaplana, D. Santamaria-Perez, O. Gomis, F. J. Manjon, J. Gonzalez, A. Segura, A. Munoz, P. Rodriguez-Hernandez, E. Perez-Gonzalez, V. Marin-Borras, V. Munoz-Sanjose, C. Drasar, V. Kucek, *Phys. Rev. B* 2011, ***84***(18), 184110(1-15).
16 L. Pauling, in *The Nature of the Chemical Bond,* Cornell University Press: Ithaca, New York, 3rd ed., 1960.
17 M. Mezouar, W. A. Crichton, S. Bauchau, F. Thurel, H. Witsch, F. Torrecillas, G. Blattmann, P. Marion, Y. Dabin, J. Chavanne, O. Hignette, C. Morawe, C. Borel, *J. Synchrotron Radiat.* 2005, ***12***, 659-664.
18 A. Dewaele, P. Loubeyre, M. Mezouar, *Phys. Rev. B* 2004, ***70***(9), 094112(1-8).
19 L. Lutterotti, S. Matthies, H. R. Wenk, A. S. Schultz, J. W. Richardson, *J. Appl. Phys.* 1997, ***81***(2), 594-600.
20 L. Lutterotti, R. Vasin, H. R. Wenk, *Powder Diffr.* 2014, ***29***(1), 76-84.
21 H. R. Wenk, L. Lutterotti, P. Kaercher, W. Kanitpanyacharoen, L. Miyagi, R. Vasin, *Powder Diffr.* 2014, ***29***(3), 220-232.
22 A. Le Bail, H. Duroy, J. L. Fourquet, *Mater. Res. Bull.* 1988**,** ***23***(3), 447-452.
23 S. Matthies, H. G. Priesmeyer, M. R. Daymond, *J. Appl. Crystallogr.* 2001, ***34***, 585-601.
24 R. J. Angel, M. Alvaro, J. Gonzalez-Platas, *Z. Kristallogr. – Cryst. Mater.* 2014, ***229***(5), 405-419.
25 R. Vilaplana, O. Gomis, F. J. Manjon, A. Segura, E. Perez-Gonzalez, P. Rodriguez-Hernandez, A. Munoz, J. Gonzalez, V. Marin-Borras, V. Munoz-Sanjose, C. Drasar, V. Kucek, V. *Phys. Rev. B* 2011, ***84***(10), 104112(1-13).
26 I. D. Bleskov, E. A. Smirnova, Y. K. Vekilov, P. A. Korzhavyi, B. Johansson, M. Katsnelson, L. Vitos, I. A. Abrikosov, E. I. Isaev, *Appl. Phys. Lett.* 2009, ***94***(16), 161901(1-3).
27 R. J. Angel, *Rev. Mineral. Geochem.* 2000, ***41***, 35-59.
28 A. Polian, M. Gauthier, S. M. Souza, D. M. Triches, J. C. de Lima, T. A. Grandi, *Phys. Rev. B* 2011, ***83***(11), 113106(1-4).
29 Z. W. Xiong, X. Y. An, Z. L. Li, T. T. Xiao, X. R. Chen, X. R., *J. Alloys Compd.* 2014, ***586***, 392-398.
30 J. R. Wiese, L. Muldawer, *J. Phys. Chem. Solids* 1960, ***15***(1-2), 13-16.

Table of contents entry

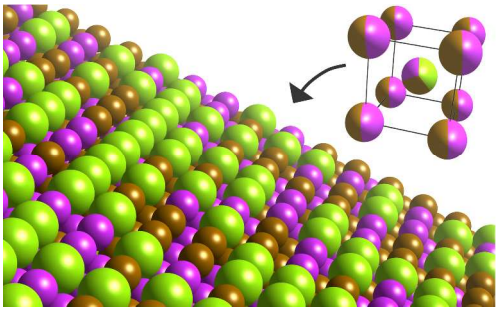

Bi_2Te_2Se appears to undergo an electronic transition near 3 GPa, then becomes a monoclinic near 10 GPa followed by a structural analogue of the cubic alloy of Bi_2Te_3 but low-angle diffraction demonstrates lower symmetry.